ELSEVIER

Journal of Nuclear Materials 303 (2002) 200–209

journal of nuclear materials

www.elsevier.com/locate/jnucmat

The reaction kinetics of lithium salt with water vapor

M. Balooch *, L.N. Dinh, D.F. Calef

Chemistry and Materials Science, Lawrence Livermore National Laboratory, P.O. Box 808, L-357, Livermore, CA 94551, USA

Received 19 November 2001; accepted 28 January 2002

Abstract

The interaction of lithium salt (LiH and/or LiD) with water vapor in the partial pressure range of 10^{-5}–2657 Pa has been investigated. The reaction probability of water with LiH cleaved in an ultra high vacuum environment was obtained using the modulated molecular beam technique. This probability was 0.11 and independent of LiH surface temperature, suggesting a negligible activation energy for the reaction in agreement with quantum chemical calculations. The value gradually reduced, however, to 0.007 as the surface concentration of oxygen containing product approached full coverage. As the film grew beyond a monolayer, the phase lag of hydrogen product increased from 0 °C to 20 °C and the reaction probability reduced further until it approached our detection limit ($\sim 10^{-4}$). This phase lag was attributed to a diffusion-limited process in this regime. For micrometer thick hydroxide films grown in high moisture concentration environment on LiD and LiH, the reaction probability reduced to $\sim 4 \times 10^{-7}$ and was independent of exposure time. In this regime of thick hydroxide films (LiOH and/or LiOD), microcracks generated in the films to release stress provided easier pathways for moisture to reach the interface. A modified microscope, capable of both atomic force microscopy and nanoindentation, was also employed to investigate the surface morphology of hydroxide monohydrate ($LiOH \cdot H_2O$ and/or $LiOD \cdot H_2O$) grown on hydroxide at high water vapor partial pressures and the kinetics of this growth.

1. Introduction

Low atomic number elements such as hydrogen, lithium and beryllium are essential parts of materials for neutron shielding applications. In ground-based reactors, water or hydrogen-containing materials are used since the weight of shielding materials is relatively unimportant. However, for applications that are weight sensitive, such as mobile nuclear reactors, lithium hydride/deuteride is an ideal material to be used for neutron shielding. The unique properties of this material include: high hydrogen content, high melting point, low dissociation pressure and low density [1]. Lithium hydride/deuteride, however, has a high affinity for water. For large quantity storage, the inadvertent reaction of the material with water generates hydrogen gas and heat, the combination of which presents potential hazards such as fire, explosion and even possibly ignition of the salt itself [2].

The interaction of water with salt was investigated more than two decades ago in some detail [3–5]. Since then, however, the efforts to understand such a complex reaction system have been missing. The early work of Machin and Tompkins [4] on single crystal LiH resulted in the finding of hydrogen production between 0 and 121 °C. The chemical nature of the solid reaction products depended on the amount of water dosed: Li_2O was formed for equivalent doses to produce a monolayer or less of the reacted product, while LiOH was the product for higher doses. In addition, they found that the introduced water was rapidly and almost completely removed from the gas phase by the solid hydride while the hydrogen-producing process continued for several hours. They also concluded that diffusion of absorbed water to the reaction interface was not the rate-controlling factor. Myers [3] used elastic proton backscattering to study the conversion of LiOH layers formed on LiH to Li_2O in the temperature of 200–280 °C. Over this temperature

* Corresponding author. Tel.: +1-925 422 7311; fax: +1-925 424 4737.

0022-3115/02/$ - see front matter
PII: S0022-3115(02)00799-7

range, Myers observed that the interaction rate was not uniform but varied by two orders of magnitude. The conversion was found to proceed via two reaction fronts, one advancing from the LiH–LiOH interface, the other from the surface. From the analysis, it was concluded that reactions at the two fronts were the limiting step in the overall process and an activation energy of 130 kJ/mol for this conversion process was deduced. No follow up report exists in the literature since the careful studies of Myers [3].

In the present work, the interaction of water molecules and vapor with salt has been investigated with a variety of techniques. The interaction of pure LiH with H_2O, up to thin LiOH coverage, was studied by molecular beam mass spectrometry. This technique is suitable for reaction probabilities determination greater than 10^{-4}. For thicker film (on the order of micrometers), where the reaction probability fell below this number, SEM and thermogravimetry (TGA) have been employed.

2. Experimental setup and results

2.1. Low exposure studies by modulated molecular beam mass spectrometry

In this technique, a modulated (i.e., synchronously chopped) beam of molecules impinges on a solid surface maintained in an ultra-high vacuum environment and the consequences of the interaction are detected by an in situ mass spectrometer which views the impingement spot. The experimental program is devoted exclusively to reactions wherein the solid is consumed by the reactant gas either via formation of volatile reaction products or growth of a non-volatile product layer at the top of the solid. The object of the experiments is to analyze the overall heterogeneous reaction in terms of elementary steps, which include adsorption (sticking) of the reactant, surface or bulk diffusion of surface intermediates, surface reaction of adsorbed species, and desorption of products. In addition to mechanistic interpretation of the reaction, the modulated molecular beam method permits quantitative determination of the rate constants of the elementary steps involved [6].

The power of the modulated molecular beam technique applied to gas–solid reactions is due principally to its ability to obtain the reaction probability and phase lag information and to the exploitation of the modulated frequency as a basic variable in addition to temperature and pressure. The reaction probability is the fraction of the incident reactant molecules which first adsorb on the surface and then leave as part of a product molecule. The phase lag of the product emission relative to the incident reactant flux is a measure of the mean lifetime of the beam species on the surface. The phase lag contains kinetic information unobtainable in conventional steady state kinetic techniques which yield only the reaction probability. In addition, the modulation technique improves the signal to noise ratio in comparison to steady state detection since the background noise can be eliminated through a lock-in detection process. The basic elements of the experimental set up are explained in detail previously [6]. In the present work, an in situ Auger electron spectroscopy (AES) has been added to monitor the reaction spot on the surface of the salt. The schematic of the experimental setup is shown in Fig. 1. The samples were cleaved in the system to assure fresh surface exposure.

Fig. 2 shows the reflected water molecules signal as a function of time as the fresh surface was exposed to 1.3×10^{-5} Pa equivalent water pressure from the molecular beam at room temperature. The reflected signal initially rose with time then leveled off after about 60 s of exposure. At this point the sample was moved to provide a fresh spot. This caused the reflected signal to drop to almost the same value as at the start of the previous cycle. The reaction probability of water, ε_{H_2O}, can be written as

$$\varepsilon_{H_2O}(t) = 1 - \frac{S_{H_2O}(t)}{S_{sat}}, \tag{1}$$

where $S_{H_2O}(t)$ is the reflected water signal at time t and S_{sat} is the reflected H_2O at the point of saturation of the surface with oxygen (i.e. full coverage). Assuming negligible reaction probability at saturation and negligible surface mobility for oxygen containing species on salt at room temperature, the reaction probability obtained from Eq. (1) is estimated to be 0.12 for the fresh surface.

The reaction probability can also be estimated by monitoring hydrogen, produced as the volatile species. This reaction probability can be written as

$$\varepsilon_{H_2O}(t) = \frac{S_{H_2(t)}}{S_{sat}} \frac{\sigma_{H_2O}}{\sigma_{H_2}}, \tag{2}$$

where σ_{H_2O} and σ_{H_2} are ionization cross sections of water and hydrogen of the mass spectrometer for conversion of signals to molecular densities. In Eq. (2), $S_{H_2}(t)$ is hydrogen signal detected at time t and S_{sat} is the hydrogen signal at the point of saturation of the surface with oxygen.

Fig. 3 shows the time dependence of the reaction probability through hydrogen detection along with oxygen coverage measured simultaneously by AES. The reaction probability of about 0.11 obtained for the fresh surface is within experimental error that was deduced earlier on by H_2O reflected signal. The probability was reduced, however, as the oxygen containing lithium compound coverage increased. For the full coverage, the probability was about 0.007. The reaction probability of 0.007 previously reported by Gregory and Mohr [7] is, thus, suspected to be on oxygen contaminated surface.

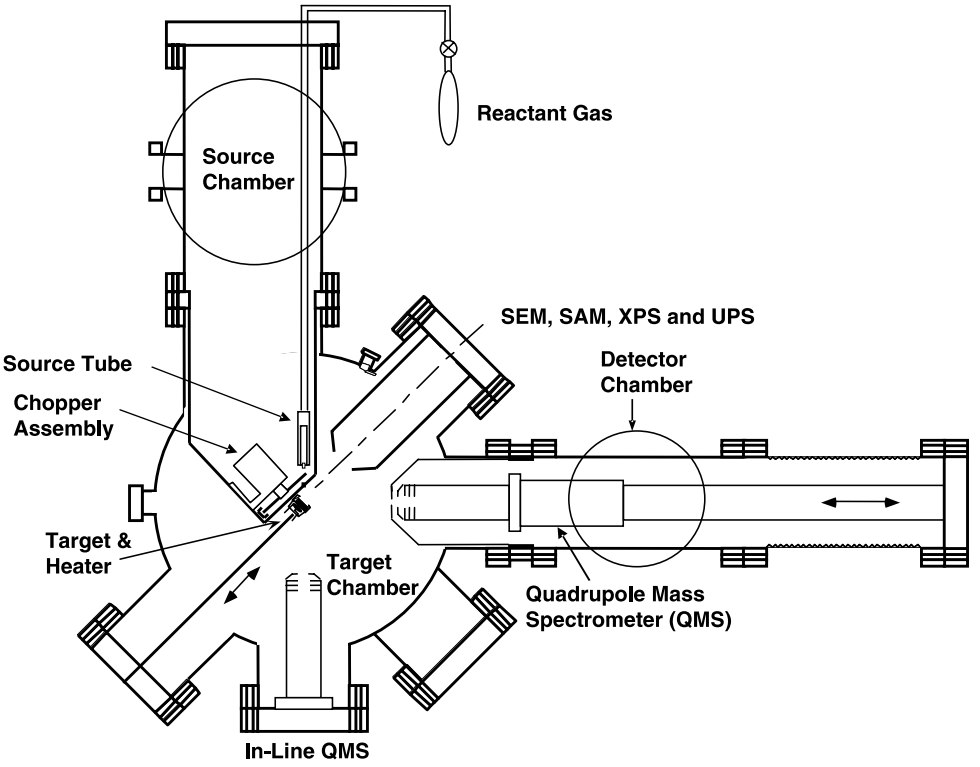

Fig. 1. Schematic of the modulated molecular beam mass spectrometry setup.

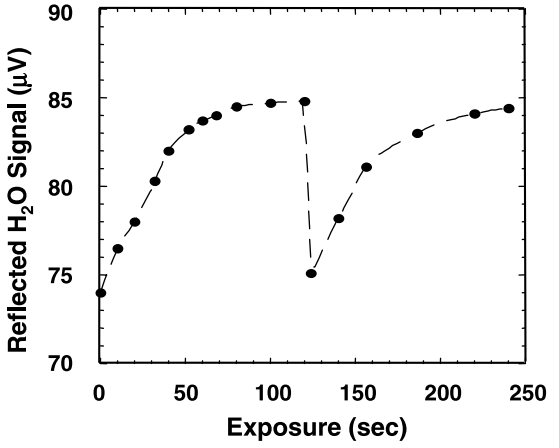

Fig. 2. The reflected water molecules signal as a function of time as the fresh LiH surface was exposed to 1.3×10^{-5} Pa equivalent water pressure.

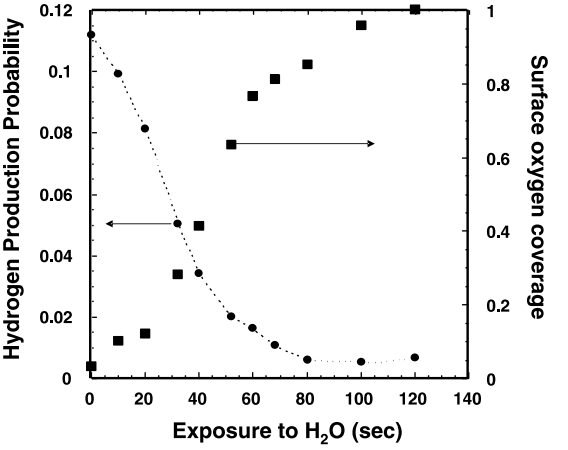

Fig. 3. The time dependence of the reaction probability through hydrogen detection along with oxygen containing species coverage measured simultaneously by AES.

The hydrogen production probability as a function of salt temperature is shown in Fig. 4. For measurement of the reaction probability at each temperature, the sample was removed to expose fresh surface to the beam. The probability is calculated from

$$\varepsilon^{T}_{H_2}(t) = \frac{S^{T}_{H_2}}{S^{300}_{H_2O}} \frac{\sigma_{H_2O}}{\sigma_{H_2}} \left(\frac{T}{300}\right)^{1/2} \left(\frac{M_{H_2O}}{M_{H_2}}\right)^{1/2}, \quad (3)$$

where $S^{T}_{H_2}$ and $S^{300}_{H_2O}$ are hydrogen and water signals at temperature T and 300 K, respectively. M_{H_2O} and M_{H_2} are molecular weights of hydrogen and water. The last

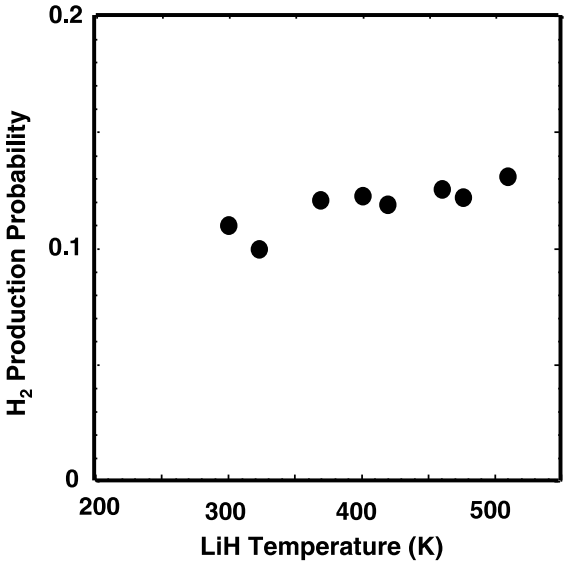

Fig. 4. Hydrogen production probability as a function of salt temperature.

two terms represent the ration of molecular velocities require for density to flux conversion in the equation. The insensitivity of the reaction probability to change with temperature suggests that the activation energy for the reaction is negligible for pure salt.

The hydrogen reaction probability and phase lag of desorbed hydrogen with respect to scattered water molecules are shown in Fig. 5, following the completion of oxygen coverage. This probability still reduced further with time while hydrogen phase lag increased to over 20 degrees. Since the interaction of water with pure

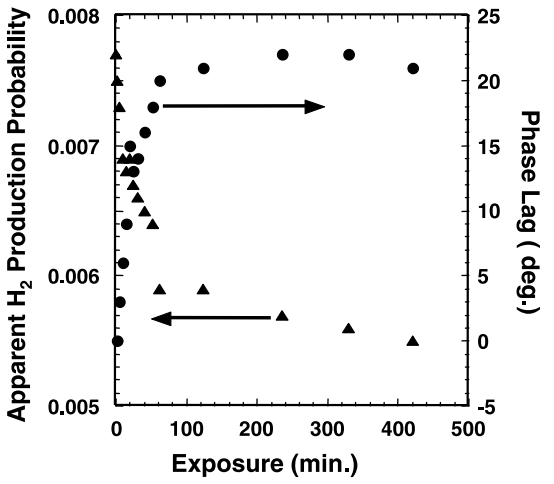

Fig. 5. The hydrogen reaction probability and phase lag of desorbed hydrogen with respect to scattered water molecules.

LiH did not produce measurable phase lag, the increase in this phase lag is attributed to the time required for oxygen containing species (H_2O, OH^-, O_2^-) to diffuse through the LiOH lattice and to react at the interface. As the thickness of the film increased, the phase lag increased along with it. This also implies that the LiOH film preserved its integrity, at least at the early stage of film growth. However, due to lattice parameter mismatch between LiH and LiOH, cracks were eventually generated to release stress as can be seen in Section 2.2.

2.2. SEM studies

In a separate experiment, a single crystal of LiD was cleaved to obtain two perpendicular {1 0 0} surfaces for SEM study. As a result of exposure to air with 50% relative humidity, the hydroxide started to grow on salt surfaces. Due to the lattice mismatch between the salt and its hydroxide (LiOH and/or LiOD), stress built up as the hydroxide film grew. At the yield point, the corners fractured to relieve stress. The dotted lines drawn in the upper part of Fig. 6 are the indications of the thicknesses where fracture took place. The growth of reaction product layers as observed by SEM is not the actual thickness since SEM measures the thickness with respect to the starting corner as shown in Fig. 6. The actual thickness, X, can be deduced by density ratio of hydroxide to LiD. The time evolution of observable hydroxide growth at 50% humidity as monitored by SEM is shown in Fig. 7. The actual hydroxide thickness, X, as a function of exposure time is shown in Fig. 8. The thickness varied linearly with exposure for films having thickness on the order of micrometers suggesting, unlike thin hydroxide film, the growth was no longer controlled by the diffusion through the hydroxide. The absence of a diffusion limitation does not necessarily imply that the lattice diffusion was rapid. The extensive microcracking of thick films during exposure offered a possible pathway for water migration to the LiD/LiOH interface [8]. The reaction probability, defined as the number of LiOH/LiOD molecules produced (estimated from the measured hydroxide thickness) to the number of water molecules striking at the surface of LiD, is around 5×10^{-7}. This value is six orders of magnitude lower than the reaction probability obtained by molecular beam analysis on bare LiH surfaces. As a result of exposing LiD to an environment with much higher moisture concentration, the formation of a product layer of hydroxide on top of the LiD surface was practically instantaneous. $LiOH \cdot H_2O$ and/or $LiOD \cdot H_2O$ were also expected to be formed on top of lithium hydroxide in an environment with >15% relative humidity [9]. After the formation of these hydroxide layers, H_2O molecules had to go through the product layers (by diffusion in thin films and through microcracks in

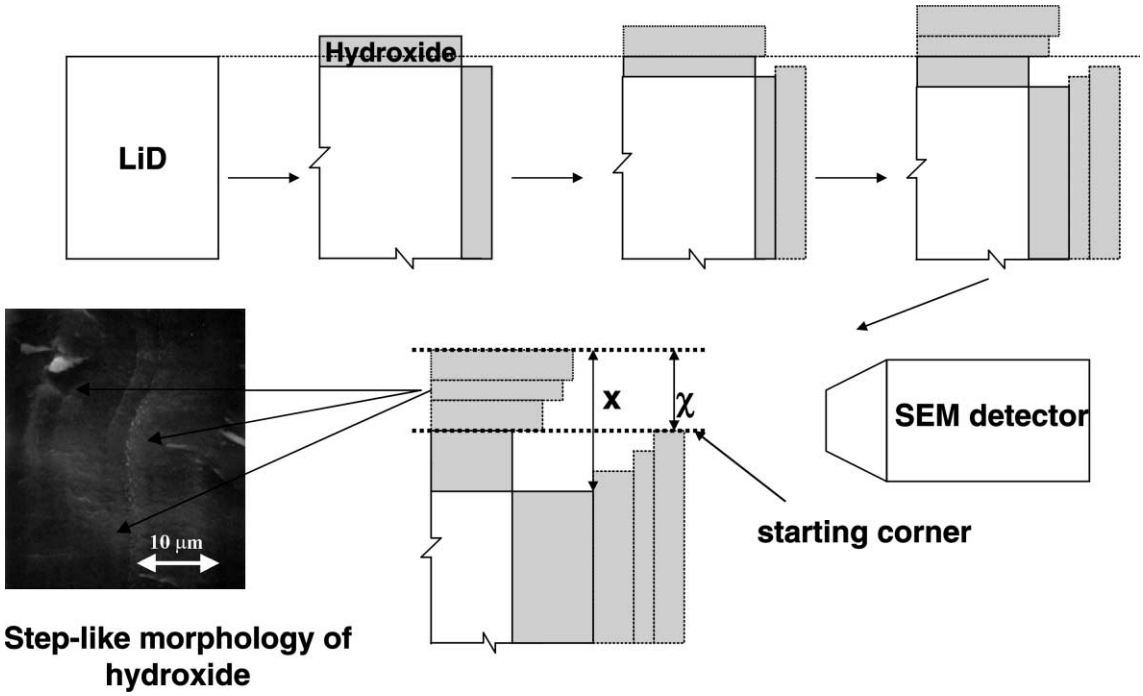

Fig. 6. Hydroxide growth pattern of single crystal LiD exposed to room air with 50% relative humidity.

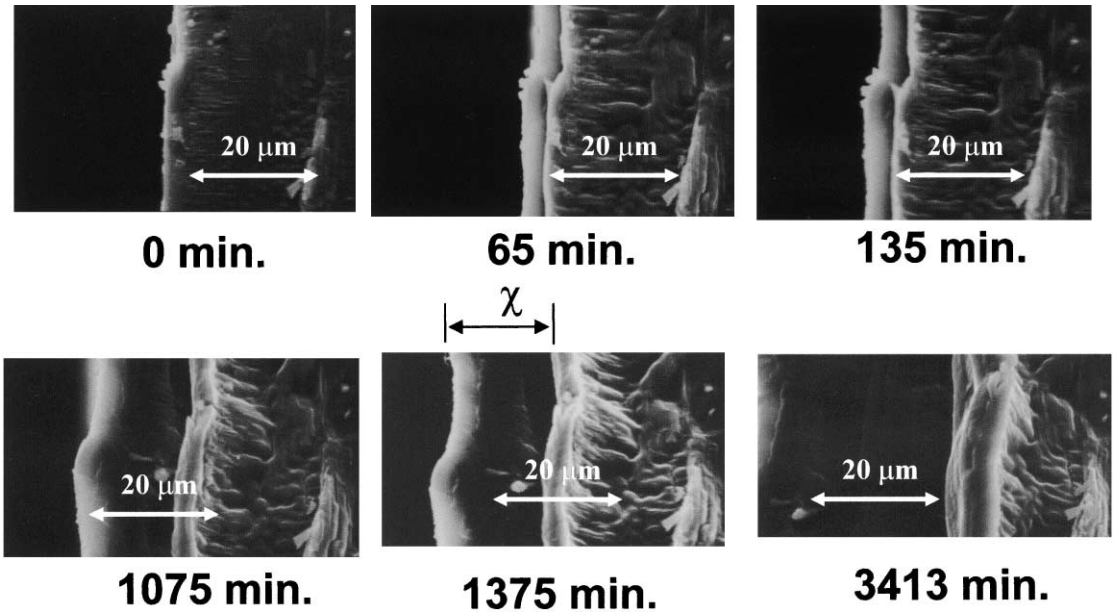

Fig. 7. Hydroxide growth at 50% relative humidity and room temperature as monitored by SEM.

thicker films) to react with LiD at the LiD/hydroxide interface. The chance for a H_2O molecule to leave the moisture saturated hydride monohydrate ($LiOH \cdot H_2O$ and/or $LiOD \cdot H_2O$) or hydroxide (LiOH and/or LiOD) surfaces after having impinged upon them was certainly much higher than in the case of a bare and reactive salt surface. This translates to a much lower reaction probability for the former case.

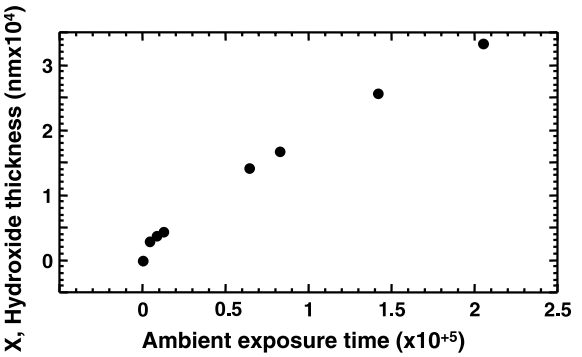

Fig. 8. Hydroxide thickness, X, as a function of moisture exposure time on LiD.

2.3. Thermogravimetric studies

The weight gain as a function of time and temperature at 100% humidity was also measured by TGA technique. The LiD single crystal slab (1 cm^2 each side) was cleaved prior to being introduced into the vacuum system which housed the microbalance for fresh surface exposure. The system was evacuated with a turbo molecular pump to about 1.3×10^{-5} Pa prior to water vapor introduction. The weight gain appeared linear with time for all temperature studied. The rate of weight gain as a function of temperature in nitrogen atmosphere saturated with water is shown in Fig. 9. The measured weight gain in time was about 0.75 mg/h at room temperature. This implies an oxygen uptake of 7.6×10^{15} atoms per second. The number of collision of H_2O molecules with the face of the sample can be obtained from kinetic theory of gases

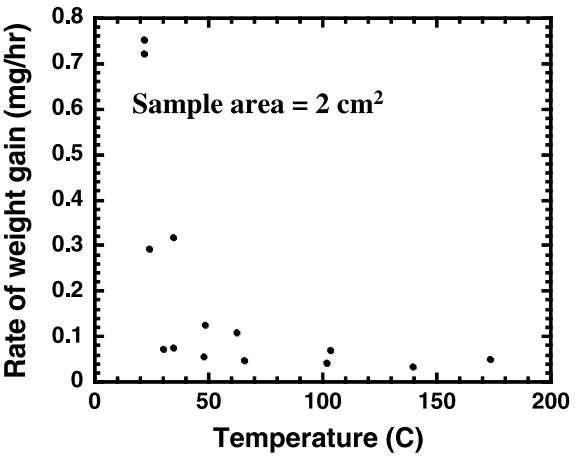

Fig. 9. The rate of weight gain of a single crystal LiD slab (1 cm^2 each side) as a function of temperature in nitrogen atmosphere saturated with water.

$$v = \frac{2.63 \times 10^{24} P\ (\mathrm{Pa})}{\sqrt{M_{H_2O} T\ (\mathrm{K})}} A\ (\mathrm{m}^2), \tag{4}$$

where P, A, T and M_{H_2O} are the water vapor pressure, surface area of the face of the sample that underwent collision with water molecules, temperature and mass of water.

For saturated water vapor, the number of collisions is about 1.7×10^{22}. Therefore the reaction probability is estimated to be 4.5×10^{-7}, in good agreement with the value determined in the SEM study. The nearly constant rate with exposure time at constant temperature suggests the lack of a diffusion-controlled process. The rate reduced, however, by a factor of ~7 as the temperature increased to 40 °C. From then on the reduction in rate became small.

To confirm the TGA result on the temperature dependence of growth, cross-sectional studies by SEM were performed on two single crystal LiD slabs at two different temperatures. Fig. 10 shows the growth of hydroxide on LiD single crystal slabs which were exposed to air at 50% relative humidity at 27 °C (sample a) and 66 °C (sample b) for 30 h. Sample a and sample b were originally from the same LiD single crystal which was subsequently cleaved into two pieces. The reacted layer from sample a and sample b were ~18–20 μm and ~3–5 μm respectively. These numbers represent a reduction in the reaction rate on the order of 4–7 as the sample temperature was raised from room temperature to 66 °C, thus confirming the TGA result.

2.4. Atomic force microscopy studies

The phase stability diagram suggests the stable product in 15% or higher humidity at room temperature is $LiOH.H_2O$ [9]. At about 60 °C, the phase transition from $LiOH \cdot H_2O$ to LiOH takes place (Fig. 11). However, at this moisture level, it appears that the formation of $LiOH \cdot H_2O$ is kinetically controlled. Smaller growth rate of this phase translates to the formation of a thin $LiOH \cdot H_2O$ film on the top of LiOH. The attempt to identify this phase with SEM failed, since as the film grew, the roughness increased accordingly. An attempt was made to measure this rate as well as mechanical properties of the films by a modified Atomic force microscopy (AFM) technique as explained below.

The AFM used in this study was a Nanoscope III (Digital Instruments, Santa Barbara, CA) with the standard head replaced with a Triboscope indentor system (Hysitron Inc., Minneapolis, MN) as previously described [10]. In this configuration the standard AFM head is replaced by a capacitive sensor. The sensor consists of two fixed outer electrodes (drive plates) that are driven by AC signals 180° out of phase relative to each other. Due to the small spacing between the two plates, the electric field changes linearly from one to the

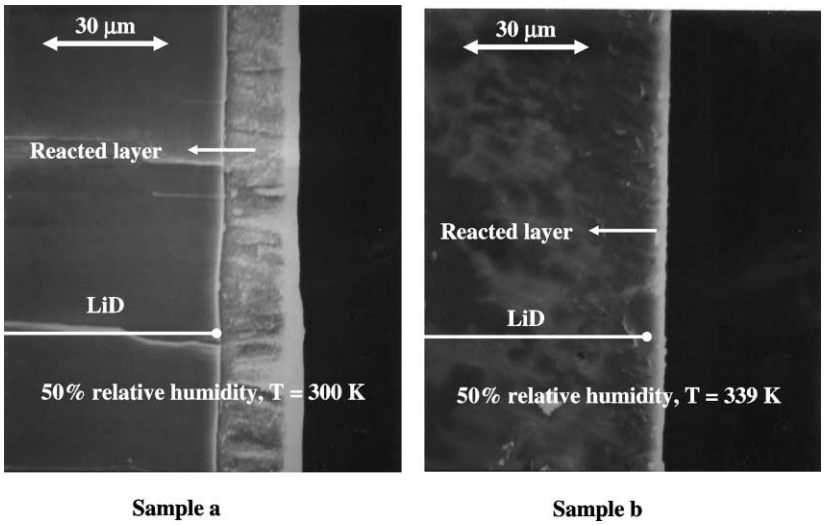

Fig. 10. The growth of hydroxide on LiD single crystal slabs which were exposed to air at 50% relative humidity at 27 °C (sample a) and 66 °C (sample b) for 30 h.

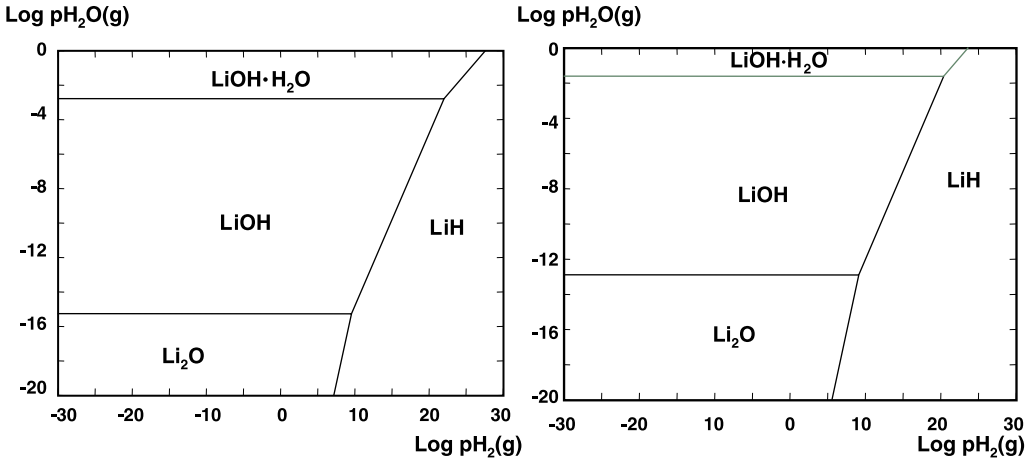

Fig. 11. Phase diagrams for LiH, Li_2O, LiOH and $LiOH \cdot H_2O$.

other. Therefore the electric field potential is maximum at the drive plates and zero at the center between the two plates. The center, or pickup, electrode is suspended in a manner that allows it to move up and down in the region between the two drive plates. The pickup electrode assumes the electric potential of the space between the two drive plates. This results in a bipolar output signal that is equal in magnitude to the input signal at the maximum deflection, and zero at the center position. The synchronous detector converts the phase and amplitude information from the sensor output into a bipolar DC output signal. The output signal is actually a reading of the pickup electrode position. In the imaging mode, this signal is used as a feedback to the piezo-ceramic tube for constant force contact imaging. In the indentation mode, the feedback is cut off and a voltage ramp is applied to the lower drive plate. As a result, an electrostatic force is generated between the pickup electrode and the drive plate. The force can be described as

$$F = k_e V^2, \tag{5}$$

where k_e is the electrostatic force constant and V is the applied voltage. The voltage ramps are formulated to produce triangular, trapezoidal or square force loading profiles of the sample. For experiments in air, the force is applied to the sample through a diamond tip glued to a tapped polymer holder attached to a pickup electrode by a small screw. In the imaging mode the minimum contact force applied to the sample is about 1 μN. In the indentation mode, load up to 30 000 μN can be applied.

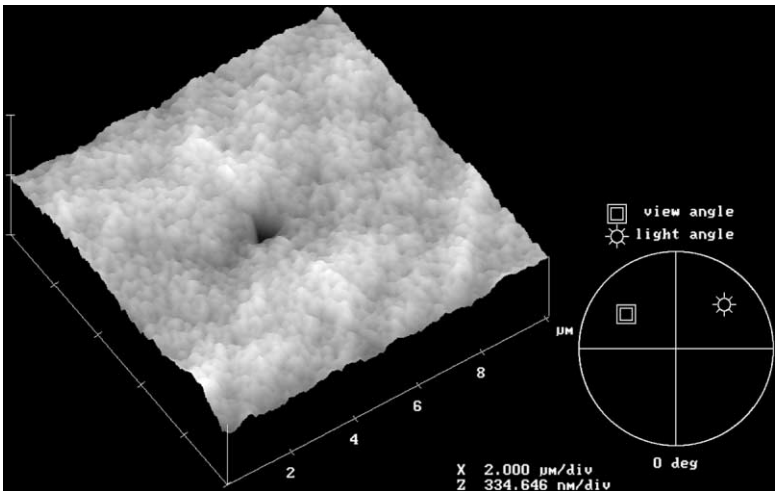

Fig. 12. The morphology and the indentation into the hydroxide monohydrate region grown on the hydroxide film developed on a LiD single crystal.

A cube corner indenter with a tip radius of curvature of about 20 nm was used for both imaging and indentation.

The hardness, H, is calculated on the basis of maximum force, F_{max}, divided by the projected contact area at maximum load, a. The elastic modulus, E, is calculated from the contact stiffness, S, defined as the slope of the linear portion of the force/displacement curve during unloading near the maximum load [11]:

$$H = \frac{F_{max}}{a}, \tag{6}$$

$$E = \sqrt{\frac{\pi}{a}}\frac{S}{2}. \tag{7}$$

Fig. 12 shows the morphology and the indentation into the hydroxide monohydrate ($LiOH \cdot H_2O$ and/or $LiOD \cdot H_2O$) region grown on the hydroxide film (LiOH and/or LiOD) after a freshly cleaved LiD sample was exposed to room air with 50% relative humidity for 5 min. The atomically smooth surface of the sample roughened with exposure time. The force–displacement curves for different exposure times at 50% relative

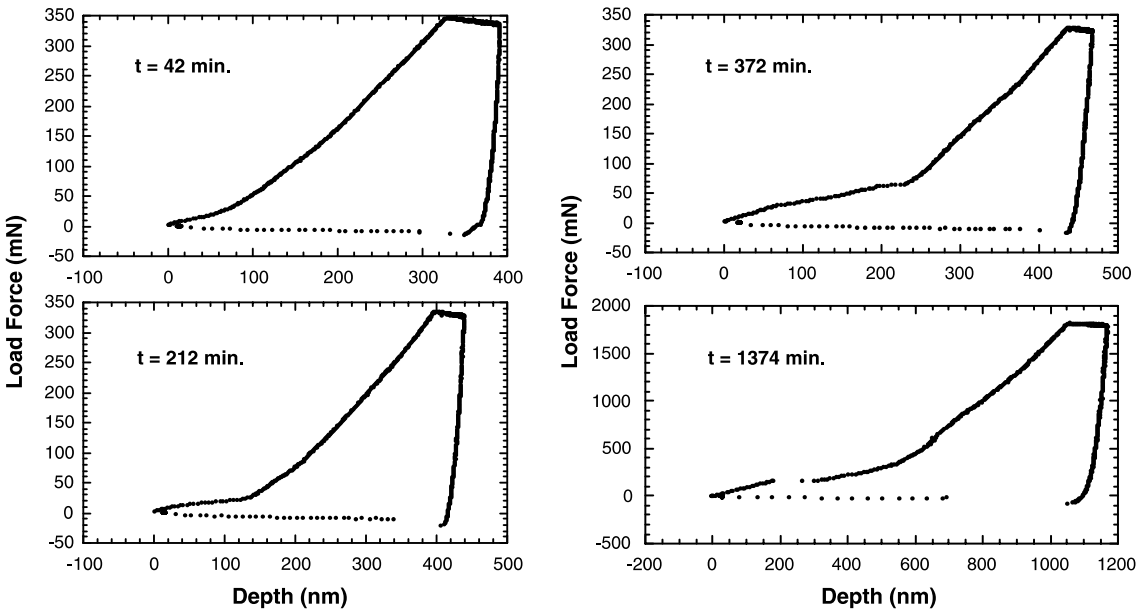

Fig. 13. The force–displacement curves for different exposure times at 50% relative humidity.

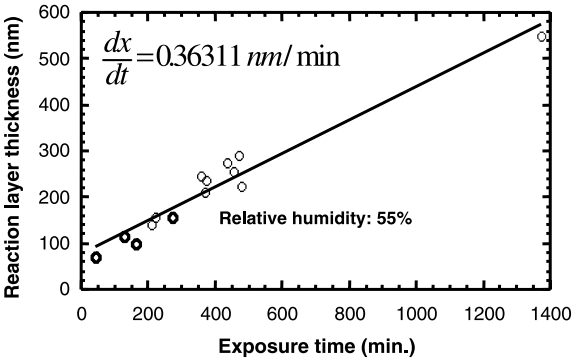

Fig. 14. The variation of the hydroxide monohydrate film thickness with exposure time.

Table 1
Elastic modulus, E, and hardness, H, of LiD, hydroxide and hydroxide monohydrate films grown on LiD

	LiD	Hydroxide	Hydroxide monohydrate
E (GPa)	40 (±3)	32 (±2)	3 (±2)
H (GPa)	1.5 (±0.2)	1 (±0.2)	0.5 (±0.2)

humidity are shown in Fig. 13. The hydroxide monohydrate film appeared to be much softer than the hydroxide film. As a result, a noticeable change in the slope was observed as the indenter penetrated through the hydroxide monohydrate/hydroxide interface. The depth at which the change of in the slope occurred is a measurement of the hydroxide monohydrate film thickness. The variation of hydroxide monohydrate film thickness with exposure time is shown in Fig. 14. The film grew linearly with time suggesting the lack of a diffusion-controlled process, as expected for such a porous film [8]. The rate of growth is calculated to be 0.363 nm/min which is a factor of 60 less than the growth of hydroxide film grown under the same conditions.

The mechanical properties of LiD, hydroxide and hydroxide monohydrate grown on LiD are summarized in Table 1 The elastic modulus of hydroxide monohydrate is an order of magnitude less than hydroxide and its hardness is a factor of two lower.

For a comparison, bulk modulus of LiH calculated from a modified Born–Mayer theory of interionic forces is 34.7 GPa [12].

3. Quantum chemical calculations

The thermodynamic barriers to simple bimolecular reactions can often be calculated using standard quantum chemical methods. Here, the reaction of a water molecule with a lithium hydride molecule was investigated. This is clearly the simplest model reaction for the experimental study of lithium hydride solid with a water vapor.

The calculations were performed using the GAMESS [14] (General Atomic and Molecular Electronic Structure System). GAMESS is a general purpose electronic structure code that supports a wide variety of basis sets and methods. Specifically, the high quality G631 basis set was employed in this report.

The calculations used the geometric optimization features of the code. An initial geometry for H_2O and LiH using classical molecular mechanics (CHEM3D) was constructed. The reactant geometry was then optimized using GAMESS by minimizing the energy. The normal, or harmonic, modes at this minimum were determined. By examining the normal modes in detail, modes that corresponded to motion of the oxygen atom toward the lithium atom were identified. The saddle point optimization feature was then utilized to search along those modes for a saddle point. Next, starting at that saddle point, the paths of steepest descent down the two sides of the saddle were found. Paths that lead down one side to reactants and the other side to the products are possible reaction pathways and the saddle point is the transition state. In general, some procedure like this is required as even a very small molecular system such as this one generates a 12-dimensional potential energy surface.

This procedure was done using two levels of theory: standard Hartree–Fock (HF) and the second order Moeller–Plesset (MP2) perturbation theory. MP2 is a correction to HF that partially incorporates the correlation effects neglected by HF. As transition state structures have unusual bonding patterns, these corrections can be important.

The results of the calculation are shown in Fig. 15. Here the calculated energy, relative to the transition

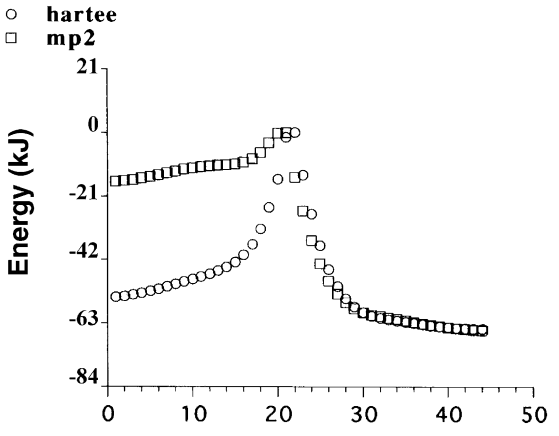

Fig. 15. Calculated energy, relative to the transition state, at 45 points along the reaction path.

state, at 45 points along the reaction path was plotted. Point 1 is $LiH + H_2O$ and point 45 is $LiOH + H_2$. At the HF level, there is a 54 kJ activation energy, but introducing the MP2 correction reduces this to 17 kJ. That relatively small number is essentially in the noise of quantum chemical calculations, so it is concluded that the barrier is extremely small. This agrees with the results of the experiment.

4. Summary and discussion

Many techniques were used to obtain insight on the LiD–water reaction system. It was found that the reaction probability is strongly influenced by the partial pressure of water, temperature and the state of LiOH and/or $LiOH \cdot H_2O$ produced.

The overall reaction rate consists of adsoption/desoption of water on the surface, transport through the hydroxide film to the LiD/LiOH interface and the reaction with salts at the interface. Any of these elementary steps can control the overall reaction rate. Adsorption depends highly on chemical composition, structure and concentration of surface impurities. The transport rate through the film can also drastically change depending on the condition of the film. For epitaxially grown films, the diffusion through the lattice controls the transport. For films grown on substrates with large lattice mismatch, cracks generated beyond a certain thickness to relieve stress in the film can provide easy pathways from the surface to the interface. This is certainly the case for the growth of micrometer thick LiOH on LiD substrate.

The reaction probability of water with pure salt was found to be 0.11 and independent of the salt temperature. Recently Broughton [13] has applied force field and quantum mechanical computational techniques to study the reaction by bringing individual water molecules to a 'slab' of lithium hydride surface. While absolute energy values have been compromised using various approximations to reduce computational time, the results confirmed that there is little or no barrier for the reaction to proceed. This is in agreement with our molecular beam and quantum chemical calculation results. The activation energy of 134 kJ/mol reported previously [2] is likely to be on oxidized surface. The reaction probability previously reported [5] of 0.007 appear also to be on oxidized surface. The results from Figs. 2 and 3 strongly support this assumption.

As thin multilayer films grow on the salt, appreciable phase lag is observed on desorbed hydrogen, suggesting that the reaction is controlled by diffusion through the film (up to some thickness). However stress builds up as the thickness of the film increases. Approaching yield stress, the film fractures to provide lower resistance pathways for transporting water to the LiD/LiOH interface.

At micron size thickness and at high concentration of water exposure (e.g. 50–100% relative humidity in air) the reaction probability further reduces to 4×10^{-7}. The rate of growth is linear with time, implying that diffusion is not the rate controlling step in this regime. One explanation for the reduction of the reaction probability in this regime as compared to thin films studied by molecular beam is the formation of $LiOH \cdot H_2O$ near the top surface as suggested by our AFM studies. If the sticking probability on $LiOH \cdot H_2O$ is smaller than LiOH, the rate limiting step could be the adsoption in this regime.

The rate of hydroxide growth drastically decreases as the temperature is increased by 30–50 °C above room temperature. With a relative humidity level of 15% or greater, thermodynamic calculations suggest a phase transition occurs between $LiOH \cdot H_2O$ and LiOH at around 50 °C. The change in sticking probability from $LiOH \cdot H_2O$ to LiOH and/or the increase in the desorption rate of water from the surface can account for the reduction in weight gain rate.

Acknowledgements

This work was performed under the auspices of the US Department of Energy by the University of California, Lawrence Livermore National Laboratory under Contract W-7405-ENG-48.

References

[1] F.H. Welch, Nucl. Eng. Des. 26 (1974) 444.
[2] J.H. Leckey, L.E. Nulf, J.R. Kirkpatrick, Langmuir 12 (1996) 6361.
[3] S.M. Myers, J. Appl. Phys. 45 (1974) 4320.
[4] W.D. Machin, F.C. Tonpkins, Trans. Faraday Soc. 62 (1966) 2205.
[5] C.E. Holcombe, G.L. Powell, J. Nucl. Mater. 47 (1973) 121.
[6] M. Balooch, D.R. Olander, J. Chem. Phys. 63 (1975) 4772.
[7] N.W. Gregory, R.H. Mohr, J. Am. Chem. Soc. 77 (1955) 2142.
[8] L.N. Dinh, C.M. Cecala, J.H. Leckey, M. Balooch, J. Nucl. Mater. 295 (2001) 193.
[9] HSC, Outokumpu Research Oy, Finland.
[10] M. Balooch, M. Wu-Magidi, I.C. Lundkvist, A.S. Balazs, S.J. Marshall, G.W. Marshall, W.J. Siekhaus, J.H. Kinney, J. Biomed. Mater. Res. 40 (1998) 539.
[11] M.F. Doerner, W.D. Nix, J. Mater. Res. 1 (1986) 601.
[12] J. Shanker, D.P. Agrawal, Phys. Stat. Sol. B 102 (1980) 495.
[13] D.A. Broughton, Technical report no. 070/99 AWE, Aldermaston, UK.
[14] M.W. Schmidt, K.K. Baldridge, J.A. Boatz, S.T. Elbert, M.S. Gordon, J.H. Jensen, S. Koseki, N. Matsunaga, K.A. Nguyen, S. Su, T.L. Windus, M. Dupuis, J.A.J. Montgomery Jr., J. Comput. Chem. 14 (1993) 1347.